Check for updates

JGR Atmospheres

RESEARCH ARTICLE
10.1029/2026JD046541

Special Collection:
Land-atmosphere coupling: measurement, modelling and analysis

Threefold Land-Use Forcing Intensifies Twofold Warming of Urban Europe

Basudev Swain[1], **Rui Song**[1], **Roy G. Grainger**[1], **and Marco Vountas**[2]

[1]NCEO; Atmospheric, Oceanic and Planetary Physics, University of Oxford, Oxford, UK, [2]Institute of Environmental Physics, University of Bremen, Bremen, Germany

Abstract Europe is warming much faster than the global average, yet the relative contributions of individual anthropogenic drivers to its urban warming remain uncertain. Using CMIP5 single-forcing simulations and observations from HadCRUT5 data set, we determine the influence of greenhouse gases (GHGs), aerosols from anthropogenic sources (Aaer), together with change in land-use (LU) forcing on urban Europe's rising surface air temperature (SAT) since 1850. The local Europe Amplification Factor (EAF), the ratio of regional to global SAT trends, reveals that LU forcing has intensified nearly threefold relative to the global mean since the industrial era, driving urban European warming almost twice the global rate. LU forcing exhibits the strongest amplification (EAF $\approx$ 3.0) compared with GHG forcing (EAF $\approx$ 2.0), highlighting the critical role of surface modifications in accelerating regional urban warming. Future projections under RCP6.0 and RCP8.5 indicate persistent EAF values exceeding 2.0 over densely populated regions, underscoring the need for integrated emission- and land-management strategies to mitigate urban Europe's amplified warming.

Plain Language Summary Europe's cities are warming faster than the global average, but the causes of this rapid increase have remained unclear. Using climate model simulations and observational data, this study examines why urban Europe is heating up more quickly than the rest of the world. We show that urban areas across Europe have warmed at nearly twice the global rate since the industrial era. In addition to greenhouse gas emissions, changes in land use, such as urban expansion and vegetation loss, strongly intensify regional warming by altering how heat is absorbed and released at the surface. When compared with global warming, land-use change produces the strongest amplification of temperature increase over Europe. Future projections indicate that this amplified warming is likely to persist throughout the century, especially under moderate to high emission scenarios and in densely populated regions. These findings highlight that limiting urban heat in Europe will require not only emission reductions, but also targeted land-use and urban planning strategies.

Key Points:

- Urban Europe warms nearly twice as fast as the global average
- Land-use change is one of the dominant amplifier of regional warming
- Amplification persists under future emission scenarios

Supporting Information:

Supporting Information may be found in the online version of this article.

Correspondence to:

B. Swain and R. G. Grainger,
basudev.swain@physics.ox.ac.uk;
don.grainger@physics.ox.ac.uk

Citation:

Swain, B., Song, R., Grainger, R. G., & Vountas, M. (2026). Threefold land-use forcing intensifies twofold warming of urban Europe. *Journal of Geophysical Research: Atmospheres*, *131*, e2026JD046541. https://doi.org/10.1029/2026JD046541

Received 28 JAN 2026
Accepted 6 OCT 2026

Author Contributions:

Conceptualization: Basudev Swain
Data curation: Basudev Swain, Rui Song
Formal analysis: Basudev Swain
Funding acquisition: Roy G. Grainger
Investigation: Basudev Swain
Methodology: Basudev Swain
Project administration: Roy G. Grainger
Resources: Roy G. Grainger
Software: Basudev Swain
Supervision: Basudev Swain, Roy G. Grainger
Validation: Basudev Swain
Visualization: Basudev Swain

© 2026 The Author(s). Journal of Geophysical Research: Atmospheres published by Wiley Periodicals LLC on behalf of American Geophysical Union. This is an open access article under the terms of the Creative Commons Attribution License, which permits use, distribution and reproduction in any medium, provided the original work is properly cited.

1. Introduction

Europe has experienced rapid and sustained urbanization over the past century, driven by industrial growth, demographic shifts, and expanding infrastructure (Quaranta et al., 2021; Shaw et al., 2020). As cities continue to expand, the accelerated rise in surface air temperature (SAT) across various continents is emerging as a vital concern in both climate science and policy (Guerreiro et al., 2018; Lauwaet et al., 2024; Swain et al., 2026; Ward et al., 2016). Unlike the global mean temperature trend, Europe is warming at a substantially faster pace, making it the fastest-warming continent according to the World Meteorological Organization (WMO) (WMO, 2022). This amplification of European warming is not merely a statistical anomaly, it carries profound implications for the occurrence and intensity of heatwaves, droughts, and other climate extremes, with cascading influence on ecosystems, and public health (Bevacqua et al., 2024; Pardo & Paredes-Fortuny, 2024; Walkowiak et al., 2025).

Demographic and socioeconomic factors further exacerbate Europe's vulnerability (Sahani et al., 2024). The combination of aging populations, declining birth rates, and migration-driven urban growth has reshaped Europe's population structure and increased vulnerability to extreme heat events (Falchetta et al., 2024; Fastl et al., 2024; Wu et al., 2025; Zanasi & Keivabu, 2024). Even with widespread economic development, capacity to adjust remains uneven-around 21.4% of Europe's population still reside in areas that cannot maintain thermal comfort in summer months (Barbosa et al., 2015; Eijkelenboom et al., 2024; Mulville et al., 2025; Santamouris & Kolokotsa, 2015). The intersection of rapid urbanization, demographic vulnerability, and accelerated warming underscores the urgency of assessing Europe's urban climate in direct relation to global temperature change.

Writing – original draft: Basudev Swain, Rui Song, Roy G. Grainger
Writing – review & editing: Basudev Swain, Rui Song, Roy G. Grainger, Marco Vountas

The drivers of this amplified warming are multifaceted, encompassing both natural variability and anthropogenic influences. Starting from the mid-19th century, globally averaged surface air temperatures have increased by about 1.09°C (Gillett et al., 2021), yet European warming has outpaced this increase (van Oldenborgh et al., 2009; WMO, 2022). Although rising greenhouse gases (GHGs) and aerosol declines under clean-air policies have been recognized as major contributors (Gavurova et al., 2021; Philipona et al., 2009; Schumacher et al., 2024), the role of land-use change, particularly urban expansion and vegetation loss, in conjunction with the effects of anthropogenic and natural forcings remains insufficiently explored over the urban regions at the continental scale. Urbanization directly modifies surface energy balance through decreased albedo, enhanced heat storage, and reduced evapotranspiration (House-Peters & Chang, 2011; Shen et al., 2021, 2023; Trlica et al., 2017), yet its contribution to urban Europe's amplified warming relative to the global mean has not been explicitly quantified.

In this study, to address this knowledge gap, we quantify the relative impacts of greenhouse gases (GHGs), aerosols from anthropogenic sources (Aaer), and modifications of land-use (LU) on the intensified surface air temperature warming over urban Europe relative to the global mean. Using the Coupled Model Intercomparison Project Phase 5 (CMIP5) (Taylor et al., 2012) ensemble of long-term single-forcing simulations, we isolate each forcing's contribution from the pre-industrial (1850–1900) to the industrial (1955–2005) periods, following IPCC SR1.5 guidelines (Masson-Delmotte et al., 2018) for defining the pre-industrial and industrial baselines. The results show that LU-driven SAT forcing over urban Europe has risen nearly threefold relative to the global mean since the industrial era, producing warming nearly twice as fast as the global average. This acceleration, enhanced by reduced aerosol cooling from clean-air policies, indicates that Europe's rapid warming is a coupled atmospheric–surface response. By situating urban European SAT trends within a global context, this study clarifies the drivers of regional urban amplification and underscores the need for integrated adaptation strategies linking emissions and land-use change.

2. Materials and Methods

This analysis is based on a comprehensive set of coupled climate model simulations drawn from the (CMIP5). Specifically, we analyze 158 simulations produced by 22 global climate models, each forced with individual anthropogenic or natural drivers (Table S1 in Supporting Information S1), covering the historical period from 1850 to 2005. These simulations are designed to reproduce observed climate evolution by explicitly prescribing external forcings such as greenhouse gas concentrations, anthropogenic aerosol emissions, volcanic activity, solar variability, and land-use change. In addition, as outlined in the IPCC Fifth Assessment Report (Taylor et al., 2012), such single-forcing experiments form the backbone of coordinated detection and attribution studies within CMIP5. The availability of individual forcing experiments differs among CMIP5 models (Table S1 in Supporting Information S1); therefore, the multi-model means for the different forcing experiments are not based on identical model ensembles. In particular, the available ensemble comprises 10 models for anthropogenic aerosol forcing, 18 models for GHG forcing, and 5 models for LU forcing. Accordingly, forcing-specific ensemble-mean responses are analyzed independently and are not summed to reconstruct the response from the combined anthropogenic forcing experiment.

In addition to historical simulations, we employ future climate projections based on monthly mean surface air temperature (SAT) from multiple representative concentration pathways (RCP2.6, RCP4.5, RCP6.0, and RCP8.5), together with historical single-forcing experiments for natural (NAT), anthropogenic aerosol (Aaer), greenhouse gas (GHG), and land-use (LU) drivers (Table S1 in Supporting Information S1). The RCP4.5 scenario represents an intermediate stabilization pathway with a radiative forcing of 4.5 W m^{-2} by 2100, corresponding to atmospheric CO_2 concentrations exceeding approximately 650 ppm, whereas RCP8.5 represents a high-emission trajectory reaching 8.5 W m^{-2} and CO_2-equivalent levels above 1,370 ppm (Van Vuuren et al., 2011).

Observed surface air temperature records were obtained from the HadCRUT5 data set (Morice et al., 2021). The SAT anomalies were calculated by subtracting the long-term pre-industrial mean (1850–1900) from area-weighted regional fields. To ensure robustness against outliers and data gaps, the median of both observational and model-derived anomalies was used in all subsequent analyses.

The urban population distribution at 1 km resolution was obtained from the Socioeconomic Data and Applications Center (SEDAC) (Gao, 2020). To ensure consistency with the climate-model fields, the high-resolution population data were aggregated to the native CMIP5 model grid (typically ∼1°) by area-weighted averaging using

21698996, 2026, 20, Downloaded from https://agupubs.onlinelibrary.wiley.com/doi/10.1029/2026JD046541 by Oxford University, Wiley Online Library on [27/10/2026]. See the Terms and Conditions (https://onlinelibrary.wiley.com/terms-and-conditions) on Wiley Online Library for rules of use; OA articles are governed by the applicable Creative Commons License

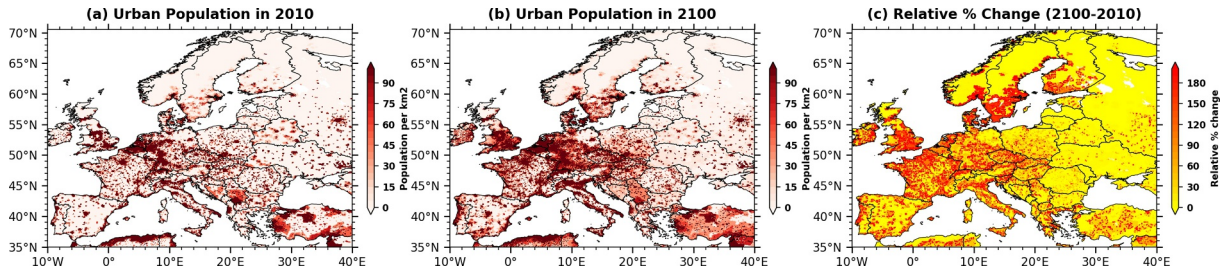


Figure 1. Current (2010) and future (2100) urban population distribution. (a and b) Urban population distribution per km^2 for 2010 and 2100, respectively. (c) The relative percentage difference between 2010 and 2100. The urban population distribution shows the rapid growth of urban expansion by 2100 over Europe.

Climate Data Operators (CDO) (Schulzweida et al., 2019), yielding a representative population distribution on each model grid. The resulting population field was used to identify the urban-influenced grid cells considered in the urban-focused analyses; these grid cells are indicated by the magenta markers/contours in the spatial figures. For urban regional averages, including the SAT anomaly time series shown in Figure 4, only these urban-influenced grid cells were included in the spatial averaging. In contrast, the colored background fields in the spatial maps show the corresponding climate variable across the full European domain and do not indicate that all colored grid cells are classified as urban. Model-simulated surface air temperature fields were analyzed on their native grids, avoiding artificial enhancement of spatial resolution. Long-term temperature trends were estimated using robust regression based on Iteratively Reweighted Least Squares (IRLS) (Holland & Welsch, 1977), which reduces sensitivity to outliers and internal variability (Kishore et al., 2016; Yang, 2013). Statistical significance of trends was assessed using Student's *t*-tests (Mishra et al., 2019), with a primary focus on the 95% confidence level.

2.1. Reasons for the Use of CMIP5 Instead of CMIP6

Although numerous studies have documented the rapid warming of Europe and its climate impacts (Gavurova et al., 2021; Philipona et al., 2009; Schumacher et al., 2024; van Oldenborgh et al., 2009; Vautard et al., 2014), the aim of this study is more specific: to quantify and attribute the historical influence of distinct anthropogenic forcings on surface air temperature changes over urban Europe at the continental scale. Achieving this objective requires the ability to disentangle the effects of greenhouse gases, anthropogenic aerosols, and land-use change-each of which alters regional climate through fundamentally different physical pathways.

The CMIP5 archive (Taylor et al., 2012) provides a consistent set of fully coupled atmosphere–ocean single-forcing simulations, including experiments driven by land-use change. Five CMIP5 models provide the LU-only experiments used in this study: CanESM2, CCSM4, GFDL-ESM2M, GISS-E2-H, and GISS-E2-R (Tables S1 and S2 in Supporting Information S1). In these experiments, LU forcing represents prescribed historical land-cover changes, including changes in forest, cropland, and pasture cover, which affect the climate response through the respective land-surface schemes by modifying surface properties and land–atmosphere exchanges of energy and moisture. Importantly, these LU-only experiments should not be interpreted as explicit simulations of urbanization. Urban canopy processes, anthropogenic heat emissions, and impervious-surface effects are not consistently represented as components of LU forcing across these models. Accordingly, the LU analysis in this study represents the response to large-scale historical land-cover change evaluated over population-defined urban-influenced regions, rather than an attribution of the temperature response specifically to urbanization or urban heat-island processes. By contrast, CMIP6 (Eyring et al., 2016) provides individual forcing experiments for greenhouse gases and anthropogenic aerosols but does not provide directly comparable fully coupled LU-only experiments required for the present analysis.

Within the CMIP6 framework, land-use influences are explored primarily through a set of sensitivity experiments (e.g., `land-hist`, `land-hist-altLu1`, and `land-hist-altLu2`) that rely on land-only model setups. While these simulations are able to represent changes in land-surface thermal states, they omit interactive coupling with the ocean and the full atmosphere, and therefore cannot capture the broader dynamical and energetic feedbacks required for robust attribution of surface air temperature changes at continental scales.

CMIP6 further offers the `hist-noLu` experiment, in which land-use conditions are held constant at pre-industrial levels (Table S2 in Supporting Information S1). Comparing this experiment with the standard

21698996, 2026, 20, Downloaded from https://agupubs.onlinelibrary.wiley.com/doi/10.1029/2026JD046541 by Oxford University, Wiley Online Library on [27/10/2026]. See the Terms and Conditions (https://onlinelibrary.wiley.com/terms-and-conditions) on Wiley Online Library for rules of use; OA articles are governed by the applicable Creative Commons License

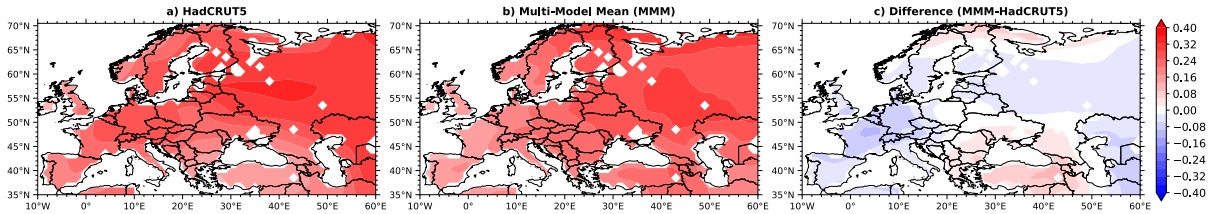


Figure 2. Spatial distribution of surface air temperature (SAT) trends over Europe from observations and model simulations for the time period from 1955 to 2005. (a) Observed SAT trends from HadCRUT5, (b) multi-model mean (MMM) SAT trends from CMIP5 simulations, and (c) the difference between model simulations and observations (MMM − HadCRUT5) for the period 1955–2005. Trends are expressed in °C decade^{-1}. The difference panel highlights regions where models underestimate (negative values) or overestimate (positive values) observed warming. The colored background represents SAT trends across the full European domain and does not denote urban classification. Magenta markers/contours indicate the urban-influenced grid cells identified from the SEDAC population distribution for 2010.

historical model estimates provides the net influence of land-use change to be inferred only indirectly, as it shows the combined response of multiple various other individual forcings. As a result, this differencing approach cannot isolate the standalone contribution of land-use change to surface air temperature trends (Figures 1a–1c).

Similarly, subtracting individual CMIP6 single-forcing experiments from the historical simulation fails to isolate LU-induced temperature responses. This discrepancy arises because temperature reactions to distinct forcing factors are not linearly additive in coupled climate models (Eyring et al., 2016; Gillett et al., 2021; Lawrence et al., 2016; Shiogama et al., 2013).

Such nonlinearity reflects complex interactions among forcing agents. For instance, aerosols modify cloud properties and radiative fluxes, thereby altering the effective warming induced by greenhouse gases, while land-use change influences surface albedo, roughness length, and soil moisture, which in turn affect atmospheric circulation and energy partitioning. These coupled feedbacks violate assumptions of linear superposition and necessitate explicit LU-only simulations to robustly quantify land-surface contributions to regional warming.

Although CMIP6 (Eyring et al., 2016) provides more recent simulations and incorporates advances in model development, the absence of directly comparable fully coupled LU-only experiments limits its application to the forcing-specific framework adopted in this study. To evaluate whether the use of CMIP5 introduces substantial differences in the historical SAT responses relevant to our analysis, we additionally compared CMIP5 and CMIP6 simulations for the forcing experiments available in both generations (Figure S4 in Supporting Information S1). The comparison includes combined anthropogenic and natural (All), total anthropogenic (Ant), anthropogenic aerosol (Aaer), greenhouse gas (GHG), and natural (NAT) forcing experiments.

The CMIP5 and CMIP6 simulations show broadly similar large-scale temporal evolution of historical SAT responses, particularly for the All, Ant, and GHG experiments, although differences in magnitude occur for individual forcings and larger differences are evident for NAT during some periods (Figure S4 in Supporting Information S1). This comparison indicates that the major historical temperature responses relevant to the present forcing analysis are broadly consistent between the two model generations. Nevertheless, CMIP6 represents a newer generation of climate models, and the comparison is not intended to establish equivalent overall model performance. CMIP5 is therefore employed here specifically because it provides an internally consistent set of fully coupled GHG-, aerosol-, and LU-only experiments required for the forcing-specific analysis, while the CMIP5–CMIP6 comparison provides an additional assessment of the robustness of the historical SAT responses for the forcing experiments available in both generations.

2.2. Estimation of the Europe Amplification Factor

To characterize the strength and spatial structure of regional warming across Europe, we computed a local Europe Amplification Factor (EAF) at each grid cell within the European domain. The EAF quantifies how strongly local surface air temperature trends depart from the corresponding global-average trend over the same period, thereby providing a spatially explicit measure of regional amplification.

For a given forcing and time interval, the EAF at location (x, y) is defined as

21698996, 2026, 20, Downloaded from https://agupubs.onlinelibrary.wiley.com/doi/10.1029/2026JD046541 by Oxford University, Wiley Online Library on [27/10/2026]. See the Terms and Conditions (https://onlinelibrary.wiley.com/terms-and-conditions) on Wiley Online Library for rules of use; OA articles are governed by the applicable Creative Commons License

$$\mathrm{EAF}(x,y) = \frac{\Delta T_{\mathrm{Europe}}(x,y)}{\Delta T_{\mathrm{global}}}, \quad (1)$$

where $\Delta T_{\mathrm{Europe}}(x,y)$ denotes the local SAT trend at that grid point, and $\Delta T_{\mathrm{global}}$ represents the globally averaged SAT trend derived from the same simulation. For consistency in regional comparisons, surface air temperature trends are evaluated over urban-influenced regions for both the European and global domains. Urban-influenced grid cells are identified from the SEDAC population distribution as described above and are indicated by magenta markers/contours in the spatial figures. The same population-based selection is applied to the European and global domains when calculating the corresponding urban SAT trends. This approach ensures that the European and global averages are derived from comparable urban-influenced regions, avoiding biases associated with mixing urban and non-urban surfaces. Consequently, the analysis isolates regional differences in warming across urban environments rather than contrasts between urban and non-urban surfaces.

For LU forcing, however, the EAF requires additional caution in its interpretation because land-use-induced temperature responses are spatially heterogeneous. Regional warming and cooling responses can partially offset each other in the global average, resulting in a relatively small global LU-induced SAT trend. Because this global trend forms the denominator of the EAF, a small global response can yield a relatively large EAF even when the absolute European LU-induced temperature trend is modest. Therefore, the LU EAF is interpreted here as a normalized diagnostic of the European response relative to the corresponding global LU response, rather than as a measure of the absolute magnitude or relative importance of LU forcing compared with other forcing agents. Accordingly, LU EAF values are interpreted together with the corresponding absolute SAT trends.

The Europe Amplification Factor is employed here as a normalized diagnostic to quantify regional temperature responses relative to the corresponding global (urban) baseline for each forcing. While LU-driven climate responses are inherently spatially heterogeneous, the EAF provides a consistent framework for assessing regional-to-global differences without implying spatial uniformity. In the CMIP5 LU-only experiments used here, LU forcing primarily represents prescribed historical land-cover transitions, including changes in forest, cropland, and pasture cover, which modify surface properties and exchanges of energy and moisture with the atmosphere (Lawrence et al., 2016). Explicit urban processes, including urban canopy effects, anthropogenic heat emissions, and impervious-surface effects, are not consistently represented as components of these LU-only experiments. Therefore, the LU EAF is interpreted as the regional response to large-scale historical land-cover forcing evaluated over population-defined urban-influenced regions, rather than as an amplification attributable specifically to urbanization or the urban heat-island effect.

This ratio-based metric facilitates direct comparison between regional and global warming rates, allowing the magnitude of European amplification to be quantified consistently across forcings. Trends were evaluated separately for the pre-industrial period (1850–1900) and the industrial period (1955–2005). All trend calculations were performed using the linear trend operator in CDO (Schulzweida et al., 2019), which applies ordinary least squares regression. To ensure statistical robustness, EAF values were computed only for grid points with statistically significant temperature trends ($p < 0.05$), while grid cells with $p > 0.05$ were excluded from further analysis. This filtering reduces the influence of internal variability and highlights spatially coherent and reliable patterns of amplification. The same procedure was applied independently to CMIP5 single-forcing simulations driven by greenhouse gases, anthropogenic aerosols, and land-use change. This approach yields forcing-specific EAF fields, enabling direct attribution of Europe's amplified warming to atmospheric composition changes versus land-surface modifications. By applying a uniform methodology across all forcings and time periods, the resulting EAF estimates are directly comparable and provide a consistent framework for interpreting both historical and future regional amplification.

3. Results

3.1. Rapidly Changing Urban Population in Europe

The spatial and temporal evolution of urban population across Europe reveals striking demographic and structural transformations with direct implications for regional surface air temperature dynamics. Using urban population data from SEDAC (Gao, 2020), we analyze the urban population distribution for 2010 and its projected state by 2100, alongside their relative percentage changes (Figures 1a–1c). The 2010 snapshot shows that Europe's urban

21698996, 2026, 20, Downloaded from https://agupubs.onlinelibrary.wiley.com/doi/10.1029/2026JD046541 by Oxford University, Wiley Online Library on [27/10/2026]. See the Terms and Conditions (https://onlinelibrary.wiley.com/terms-and-conditions) on Wiley Online Library for rules of use; OA articles are governed by the applicable Creative Commons License

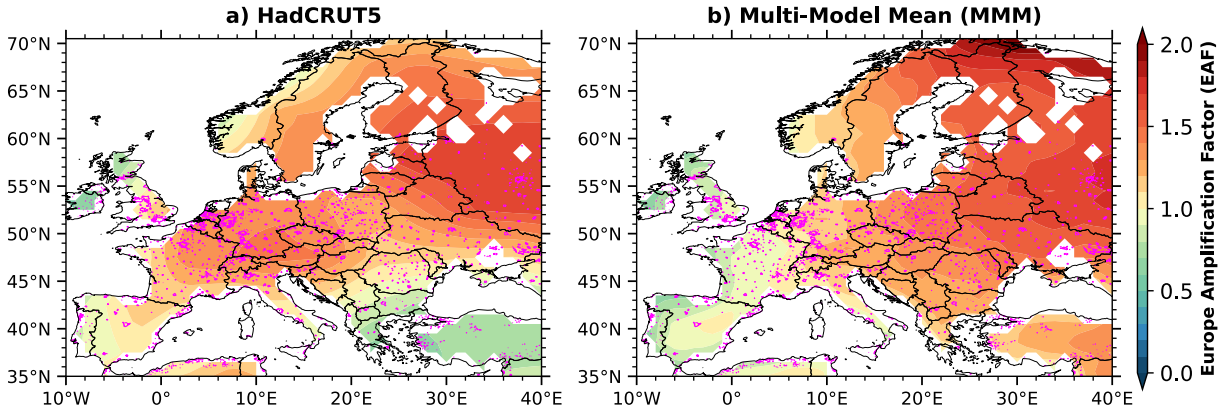


Figure 3. Spatial distribution of the Europe Amplification Factor (EAF) derived from observations and model simulations. (a) EAF calculated from HadCRUT5 observations and (b) EAF from the CMIP5 multi-model mean (MMM) for the period 1955–2005. The EAF represents the ratio of regional to global (urban) surface air temperature trends. Values greater than unity indicate amplified warming relative to the global baseline, while values below unity indicate weaker regional warming. The colored background represents EAF values across the full European domain and does not denote urban classification. The colored background represents EAF values across the full European domain and does not denote urban classification. Magenta markers indicate the urban-influenced grid cells identified from the SEDAC population distribution for 2010.

population is highly concentrated within a few densely populated belts, most notably the Rhine–Ruhr industrial corridor in Germany, the Benelux region, northern Italy's Po Valley, and the Paris metropolitan area (Figure 1a). These regions constitute Europe's economic and infrastructural cores and represent areas where anthropogenic heat fluxes and land-surface modification are already significant. In contrast, urban population expansion in Eastern and Northern Europe remains spatially fragmented, characterized by smaller, scattered urban centers embedded within extensive rural landscapes (Figure 1a).

Projections for 2100 indicate both a quantitative expansion in population density and a qualitative transformation of the urban landscape (Figure 1b). Central and eastern European cities are projected to expand outward, merging into contiguous megacity regions, while Western and Southern Europe exhibit substantial urban sprawl along coastlines and transportation corridors. Even Northern Europe, historically less urbanized, shows pronounced relative growth in urban share, likely driven by migration-induced demographic shifts (Figure 1c). Collectively, these transformations suggest that by 2100, approximately 90%–150% more people will inhabit urban areas compared to 2010, and urbanized land surfaces will dominate the European continental climate system.

At finer spatial scales, the 1 km-resolution data reveal substantial heterogeneity in the trajectories of urban growth. While existing large metropolitan centers continue to attract the majority of new residents, mid-sized cities and peri-urban zones-especially across Eastern and Southern Europe-are expected to absorb a growing share of the population (Figures 1a and 1b). This secondary urbanization process represents an emerging and climatically relevant phenomenon. This expands the spatial footprint of anthropogenic heat sources and intensifies regional land-use forcing. The resulting modification of land-surface characteristics can alter vegetation cover, surface radiative properties, evapotranspiration, and turbulent heat exchange, thereby modifying local surface energy and moisture fluxes. Consequently, these demographic transformations are not merely socio-economic developments but active drivers of Europe's regional climate system, serving as both indicators and amplifiers of future SAT change.

3.2. Europe Warming Estimated by Model and Observations

The spatial distribution of SAT trends during the industrial period reveals both broad consistency and important divergences between observations and model simulations (Figures 2a–2c). The observational data from HadCRUT5 reveal a spatially heterogeneous warming pattern across Europe (Figure 2a). The highest SAT trends $(\geq 0.40\ ^{\circ}\mathrm{C\,decade^{-1}})$ are concentrated over northeastern Europe, while central Europe exhibits moderately elevated trends ($0.32\ ^{\circ}\mathrm{C\,decade^{-1}}$). In contrast, southern regions, including the Iberian Peninsula, show comparatively weaker warming signals. Northern Italy and parts of central Europe nevertheless display notable warming, reflecting the combined influence of radiative forcing and land-surface feedbacks. By contrast, the CMIP5 multi-model mean (MMM) captures the large-scale warming pattern but with diminished spatial

21698996, 2026, 20, Downloaded from https://agupubs.onlinelibrary.wiley.com/doi/10.1029/2026JD046541 by Oxford University, Wiley Online Library on [27/10/2026]. See the Terms and Conditions (https://onlinelibrary.wiley.com/terms-and-conditions) on Wiley Online Library for rules of use; OA articles are governed by the applicable Creative Commons License

21698996, 2026, 20, Downloaded from https://agupubs.onlinelibrary.wiley.com/doi/10.1029/2026JD046541 by Oxford University, Wiley Online Library on [27/10/2026]. See the Terms and Conditions (https://onlinelibrary.wiley.com/terms-and-conditions) on Wiley Online Library for rules of use; OA articles are governed by the applicable Creative Commons License

variability and muted extremes (Figure 2b). The difference field (MMM – HadCRUT5) emphasizes these discrepancies, showing that observed SAT trends exceed simulated values by ∼0.05–0.16 °C decade^{-1} over many regions of western and central Europe (Figure 2c). These discrepancies align closely with major urban agglomerations, including the Rhine–Ruhr metropolitan region, the Benelux corridor, Paris, and northern Italy's Po Valley (Figure 2c). This spatial correspondence indicates that CMIP5 models, operating at relatively coarse spatial resolution and lacking explicit urban land-surface parameterizations, systematically underestimate SAT trends in heavily urbanized regions. The mismatch highlights the role of localized processes-such as altered surface albedo, anthropogenic heat emissions, and reduced evapotranspiration-that are not adequately captured by global climate models but critically shape regional temperature responses. Although CMIP5 models do not explicitly resolve urban canopy processes or anthropogenic heat fluxes, land-use forcing is represented through changes in surface properties such as albedo, vegetation cover, and evapotranspiration (Lawrence et al., 2016; Shiogama et al., 2013). These parameterizations capture the dominant biogeophysical effects of land transformation at the grid scale. Accordingly, our analysis targets large-scale land-use–driven temperature responses, and the results should be interpreted as regional amplification associated with land-use change rather than explicit urban heat island processes.

Further insight into Europe's warming divergence from the global mean is provided by the Europe Amplification factor (EAF), which quantifies local amplification relative to global SAT trends. The observationally derived EAF (Figure 3a) shows a spatially heterogeneous amplification pattern across Europe. Central Europe exhibits moderate amplification with values generally reaching up to ∼1.5, while eastern Europe displays somewhat higher values approaching ∼1.8. In contrast, southern regions, including the Iberian Peninsula and southeastern Europe, show relatively weaker amplification, with EAF values close to unity. Western Europe is characterized by modest amplification (∼1.0–1.5), whereas northern Europe exhibits spatially variable but overall positive EAF values. While regions of enhanced amplification often occur in areas with substantial urbanization and land modification, the figure does not provide sufficient evidence for a robust quantitative relationship between EAF and urban density. The MMM-simulated EAF pattern (Figure 3b) captures the broad spatial distribution of amplification across Europe, but underestimates the magnitude of peak values by approximately 0.3–0.6 compared to observations. In particular, the model shows relatively higher EAF values over southeastern Europe and lower values over western Europe, consistent with the spatial differences relative to HadCRUT5. The discrepancies between the model and observations are not confined to urban regions, suggesting that the underestimation arises from broader regional-scale processes rather than exclusively from urban land-use effects.

3.3. Impact of Different Forcings on Urban Europe SAT Temporal Evolution

The temporal evolution of SAT anomalies over urban Europe reveals a clear anthropogenic imprint, with distinct phases of warming corresponding to different forcings (Figures 4a–4f). Over regions with urban population distribution, observational records (HadCRUT5) display a gradual increase in SAT anomalies relative to the pre-industrial baseline until the mid-20th century, followed by a sharp acceleration after 1970 (Figure 4a). This acceleration coincides with the era of rapid industrial growth, increasing greenhouse gas (GHG) concentrations, and widespread urban expansion. The ensemble mean of combined anthropogenic and natural forcings reproduces the observed temporal evolution, indicating that external drivers dominate the evolution of urban European SAT (Figures 4b–4f).

Disentangling the contributions of individual forcings reveals that GHG forcing produces the dominant long-term warming signal (Figure 4d). The GHG-induced anomaly increases steadily throughout the industrial era, with a pronounced rise after 1950, consistent with the observed global acceleration in CO_2 and CH_4 concentrations (Etheridge et al., 1996). In contrast, anthropogenic aerosols exert a compensating cooling influence during the mid-20th century (Figure 4c), particularly over industrialized and densely populated regions. Aerosol-induced cooling temporarily offsets the GHG-driven warming, lowering net SAT trends by up to ∼0.15 °C decade^{-1} in several regions. This effect weakens substantially after the implementation of European clean-air policies in the 1970s and 1980s, allowing the full magnitude of GHG forcing to dominate.

Land-use (LU) change exerts an additional, spatially heterogeneous influence on urban SAT anomalies (Figure 4e). The LU contribution strengthens during the industrial period, reflecting the increasing influence of large-scale land-cover transformations represented in the CMIP5 LU-only experiments. These transformations modify the surface energy balance through changes in surface radiative properties, evapotranspiration, and

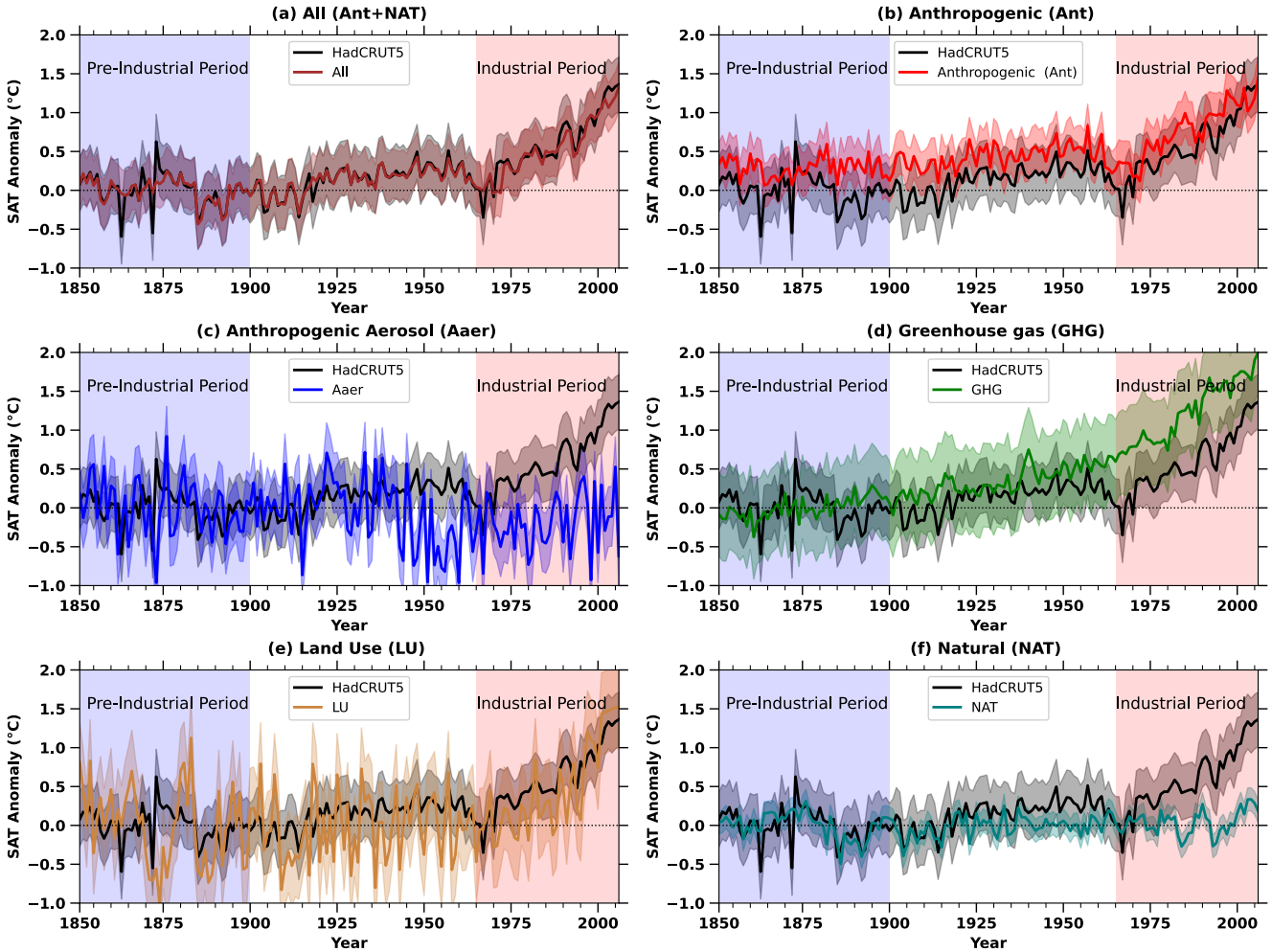


Figure 4. Temporal evolution of surface air temperature (SAT) anomalies under different forcing drivers in urban Europe. Annual SAT anomalies from observations (HadCRUT5) and model simulations are shown for (a) combined anthropogenic and natural forcings (All), (b) anthropogenic forcing (Ant), (c) anthropogenic aerosols (Aaer), (d) greenhouse gases (GHG), (e) land-use change (LU), and (f) natural forcing (NAT). Anomalies are computed relative to the 1850–1900 baseline climatology. Shaded regions denote the pre-industrial (1850–1900) and industrial (1955–2005) periods. The time series represent spatial averages calculated only over the urban-influenced grid cells identified from the SEDAC population distribution for 2010 (corresponding to the urban regions indicated by magenta markers/contours in the spatial figures), rather than over all grid cells within the European domain. The forcing-specific time series represent independent coupled-model experiments and are based on the available model ensemble for each forcing (Table S1 in Supporting Information S1). Consequently, the individual GHG, Aaer, and LU ensemble-mean responses should not be arithmetically summed to reconstruct the total anthropogenic (Ant) response.

turbulent heat exchange. The resulting SAT response is therefore spatially heterogeneous and reflects the combined effects of changes in surface albedo and the partitioning of available energy between latent and sensible heat fluxes. Quantitatively, GHG forcing accounts for mean SAT trends of approximately 0.4 °C decade^{-1} over urban Europe during the industrial period, while LU forcing contributes ∼0.15–0.25 °C decade^{-1}, depending on region. Natural forcings (volcanic and solar) fail to reproduce the observed post-1950 warming trajectory (Figure 4f).

Taken together, the individual forcing experiments illustrate distinct temperature responses associated with GHG, anthropogenic aerosol, and LU forcing. These forcing-specific responses should not be interpreted as additive components of the total anthropogenic simulation because they arise from independent coupled-model experiments and, at the multi-model-mean level, are derived from different subsets of available CMIP5 models (Table S1 in Supporting Information S1). The total anthropogenic response therefore represents the coupled climate response to the combined forcing experiment rather than the arithmetic sum of the ensemble-mean individual forcing responses shown in Figure 4.

21698996, 2026, 20, Downloaded from https://agupubs.onlinelibrary.wiley.com/doi/10.1029/2026JD046541 by Oxford University, Wiley Online Library on [27/10/2026]. See the Terms and Conditions (https://onlinelibrary.wiley.com/terms-and-conditions) on Wiley Online Library for rules of use; OA articles are governed by the applicable Creative Commons License

3.4. Anthropogenic Influence on Europe Amplification Factor (EAF)

The spatial patterns of the Europe Amplification Factor (EAF) for different climate forcings during the pre-industrial and industrial periods provide a comprehensive view of how human and natural drivers have shaped Europe's regional temperature response (Figures 5ia–5ie and 5iia–5iie). Each panel illustrates the EAF, computed as the ratio of local to global SAT trends for individual forcings, with white areas denoting statistically insignificant trends. This metric offers an explicit spatial measure of how strongly local European warming diverges from global mean temperature trends. The significant surface air temperature trends associated with each natural and anthropogenic forcing are presented in Figure S1 in Supporting Information S1.

During the pre-industrial period, amplification across Europe was generally weak, spatially fragmented, and largely governed by natural variability (Figures 5ia–5ie). Under anthropogenic forcing (Figure 5i-a), EAF values remain insignificant, suggesting negligible deviation from the global mean. Natural forcing (Figure 5i-b) produces slightly higher amplification (≈1.5–2) over northern Europe, reflecting modest sensitivity to volcanic and solar variability during this era. A faint but discernible greenhouse signal emerges under GHG forcing (Figure 5i-c), with localized enhancement over parts of northern and western Europe, though overall amplification remains limited. Land-use (LU) forcing (Figure 5i-d) displays low and insignificant spatially discontinuous amplification (<1.0–1.1), consistent with the minimal extent of anthropogenic land modification prior to industrialization. In contrast, aerosol (Aaer) forcing (Figure 5i-e) exhibits weak negative amplification (<1.0) across southern and eastern Europe, reflecting early, localized aerosol-induced cooling effects. Collectively, these patterns confirm that during the pre-industrial era, natural processes dominated Europe's climate variability, with anthropogenic influences still nascent and regionally constrained. In addition, relatively higher EAF values are observed over northern Europe, indicating enhanced regional warming compared to the global (urban) baseline. This amplification is consistent with increased high-latitude climate sensitivity like Arctic Amplification (Swain et al., 2026; Wendisch et al., 2023), driven by processes such as snow–albedo feedback, reduced influence of nearby sea-ice variability, and stronger land–atmosphere coupling.

The industrial period exhibits a clear emergence of spatially structured amplification across Europe (Figures 5iia–5iie). Under anthropogenic forcing (Figure 5ii-a), amplification is not spatially uniform: eastern Europe shows elevated EAF values, reaching up to ∼1.6, while western Europe exhibits weaker amplification, with values close to or below unity. This indicates stronger regional warming relative to the global (urban) baseline in the eastern part of the continent. Natural forcing (Figure 5ii-b) remains weak (<1.2), confirming its limited contribution to recent warming patterns. The GHG forcing pattern (Figure 5ii-c) shows a similar spatial structure, with higher amplification over eastern Europe and comparatively lower values over western regions, highlighting the dominant role of greenhouse gases while also reflecting regional differences in climate response.

The LU forcing distribution (Figure 5ii-d) exhibits a particularly striking amplification pattern. The EAF values exhibit a west–east gradient, with western Europe showing values close to or below unity, while eastern Europe displays substantially higher amplification. In particular, large areas in eastern Europe exhibit EAF values exceeding ∼2.0, indicating stronger regional warming relative to the global (urban) baseline. Central and southeastern Europe show intermediate amplification, reflecting spatial variability in the response to land-use forcing. This strong amplification highlights the profound impact of surface transformations-urban expansion, deforestation, and agricultural intensification-on local climate. These processes reduce surface albedo, suppress evapotranspiration, and enhance heat storage in built environments, thereby elevating near-surface temperatures relative to the global mean. In some regions, such as parts of central and eastern Europe, higher urban population influence coincides with modestly elevated EAF values at the grid scale, although no systematic association is evident across the domain. Conversely, the Aaer forcing pattern (Figure 5ii-e) maintains localized, very little cooling signatures, with EAF values nearly unity across western Europe, indicative of less aerosol masking of greenhouse warming due to clean air policies.

To further investigate the physical processes associated with the LU-induced SAT response, we examined changes in surface albedo and turbulent heat fluxes in the CMIP5 LU-only simulations (Figures S5–S7 in Supporting Information S1). Surface albedo exhibits spatially heterogeneous trends during the industrial period, with both increases and decreases across Europe (Figure S5 in Supporting Information S1), demonstrating that the LU response cannot be characterized by a uniform reduction in albedo. The latent heat flux response is similarly heterogeneous, with decreasing trends over parts of central and southeastern Europe and increasing trends in other regions (Figure S6 in Supporting Information S1). In contrast, sensible heat flux exhibits widespread positive

21698996, 2026, 20, Downloaded from https://agupubs.onlinelibrary.wiley.com/doi/10.1029/2026JD046541 by Oxford University, Wiley Online Library on [27/10/2026]. See the Terms and Conditions (https://onlinelibrary.wiley.com/terms-and-conditions) on Wiley Online Library for rules of use; OA articles are governed by the applicable Creative Commons License

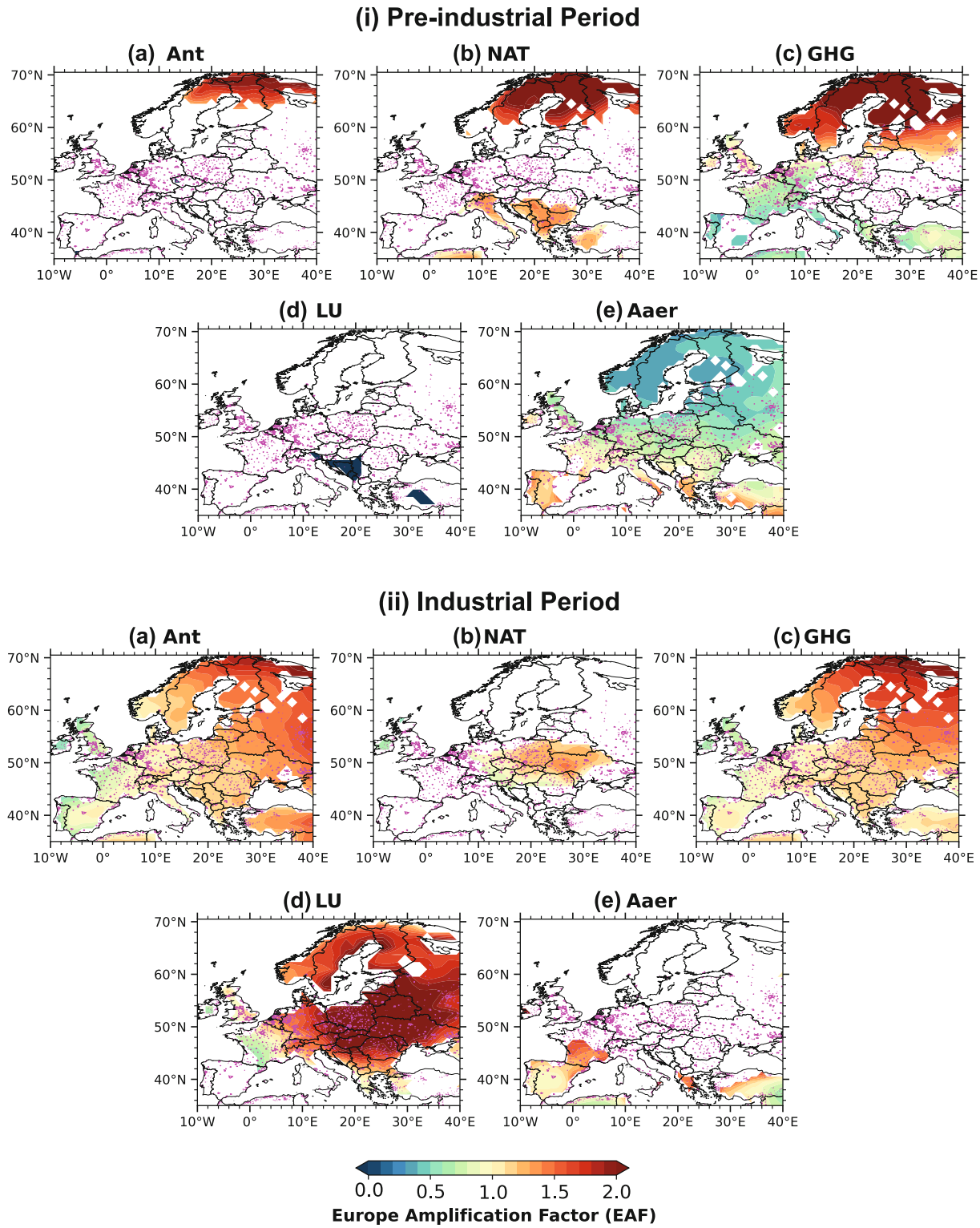


Figure 5. Spatial distribution of the Europe Amplification Factor (EAF) for different forcings during the pre-industrial and industrial periods. (i) Pre-industrial period (1850–1900) and (ii) industrial period (1955–2005) EAF patterns for (a) total anthropogenic forcing (Ant), (b) natural forcing (NAT), (c) greenhouse gases (GHG), (d) land-use change (LU), and (e) anthropogenic aerosols (Aaer). The EAF is defined as the ratio of regional to global (urban) surface air temperature trends. Values greater than unity indicate amplified regional warming relative to the global baseline, while values below unity indicate weaker responses. The colored background represents EAF values across the full European domain and does not denote urban classification. Magenta markers indicate the urban-influenced grid cells identified from the SEDAC population distribution for 2010.

21698996, 2026, 20, Downloaded from https://agupubs.onlinelibrary.wiley.com/doi/10.1029/2026JD046541 by Oxford University, Wiley Online Library on [27/10/2026]. See the Terms and Conditions (https://onlinelibrary.wiley.com/terms-and-conditions) on Wiley Online Library for rules of use; OA articles are governed by the applicable Creative Commons License

21698996, 2026, 20, Downloaded from https://agupubs.onlinelibrary.wiley.com/doi/10.1029/2026JD046541 by Oxford University, Wiley Online Library on [27/10/2026]. See the Terms and Conditions (https://onlinelibrary.wiley.com/terms-and-conditions) on Wiley Online Library for rules of use; OA articles are governed by the applicable Creative Commons License

trends across substantial parts of Europe during the industrial period (Figure S7 in Supporting Information S1). Together, these changes indicate that the LU-induced SAT response is associated with spatially varying modifications of the surface energy balance, including changes in radiative properties and the partitioning of available energy between latent and sensible heat fluxes, rather than a single uniform albedo-driven mechanism.

Overall, the transition from the pre-industrial to the industrial era signifies a fundamental reorganization of the European amplification landscape-from weak, spatially inconsistent signals to a robust, continent-wide pattern dominated by anthropogenic influence (Figures 5i and 5ii). The Europe Amplification Factor strengthens most prominently under anthropogenic, GHG, and LU forcings, with urban and land-modified regions showing the highest local amplification. These results underscore that human-induced surface and atmospheric changes-particularly those associated with land-use transformation-play a decisive role in shaping urban Europe's enhanced warming relative to the global mean.

Further insight into this amplification emerges when comparing the changes of significant SAT trends for urban Europe and global urban regions during the pre-industrial and industrial periods (Figures 6a and 6b). During the pre-industrial era (Figure 6a), both European and global SAT trends remain small and statistically weak, typically within -0.1–$0.1\ ^{\circ}\mathrm{C\ decade}^{-1}$ across all forcings. Slightly positive but modest warming occurs under GHG forcing $(\approx 0.05$–$0.1\ ^{\circ}\mathrm{C\ decade}^{-1})$, while LU and Aaer forcings exhibit negative or near-zero values, resulting in negligible amplification. The weak cooling signal associated with land-use forcing during the pre-industrial period likely reflects limited and spatially heterogeneous land-cover changes. Early deforestation and agricultural expansion can increase surface albedo and reduce net radiation, leading to slight cooling. Given the small magnitude of land-use forcing during this period, these trends are modest and may also be influenced by internal variability. The corresponding EAF values hover near unity ($\approx$1.0), confirming minimal divergence between urban Europe and the global mean during this early period.

In contrast, the industrial period (Figure 6b) reveals a marked intensification of warming, particularly over urban European regions. Average SAT trends over Europe reach approximately 0.4–0.5 $^{\circ}\mathrm{C\ decade}^{-1}$ under anthropogenic and GHG forcings, compared with global urban trends of approximately 0.2–0.3 $^{\circ}\mathrm{C\ decade}^{-1}$. The LU experiment yields a comparatively large EAF of approximately 3, indicating that the LU-induced SAT response over urban Europe is substantially stronger relative to the corresponding global-mean LU response. However, LU forcing produces spatially heterogeneous warming and cooling responses, which can partially compensate when averaged over the global urban domain, resulting in a relatively small global-mean LU SAT trend. Consequently, the magnitude of the LU EAF is sensitive to this small global denominator and should not be interpreted as indicating that LU produces a larger absolute warming contribution than GHG forcing. Indeed, the absolute SAT trends in Figure 6b show that the European temperature response to GHG forcing is substantially larger than that associated with LU forcing. The high LU EAF therefore indicates a pronounced regional contrast between the European and global responses to land-use forcing, rather than a ranking of the absolute contributions of different forcing agents to European warming. Aerosol forcing exhibits a comparatively weak regional-to-global contrast during the industrial period.

3.5. Future Projections of Europe Warming

The spatial distribution of the Europe Amplification Factor under different Representative Concentration Pathways (RCPs) from 2010 to 2100 provides a comprehensive view of how regional amplification is projected to evolve under varying emission trajectories (Figures 7a–7d). Panels (a–c) correspond to RCP2.6, (d–f) to RCP4.5, (g–i) to RCP6.0, and (j–l) to RCP8.5, corresponding to the early (2010–2039), intermediate (2040–2069), and late (2070–2099) future time horizons, respectively. The urban regions (magenta circles) where amplification has been explicitly evaluated, highlighting the spatial coupling between population density and regional SAT amplification. The significant surface air temperature (SAT) trends for different RCP scenarios across the various future periods are presented in Figure S2 in Supporting Information S1.

Across all scenarios, the near-future projections (2010–2039) show moderate amplification over the European continent, with EAF values generally ranging between $\sim$0.8 and 1.5. Under the low-emission RCP2.6 scenario (Figure 7a), mild amplification appears across central and northern Europe, whereas southern regions exhibit weak EAF values, consistent with limited additional warming under strong mitigation and relatively stable radiative forcing. Similar but slightly intensified patterns are observed for RCP4.5 and RCP6.0 (Figures 7d and 7g),

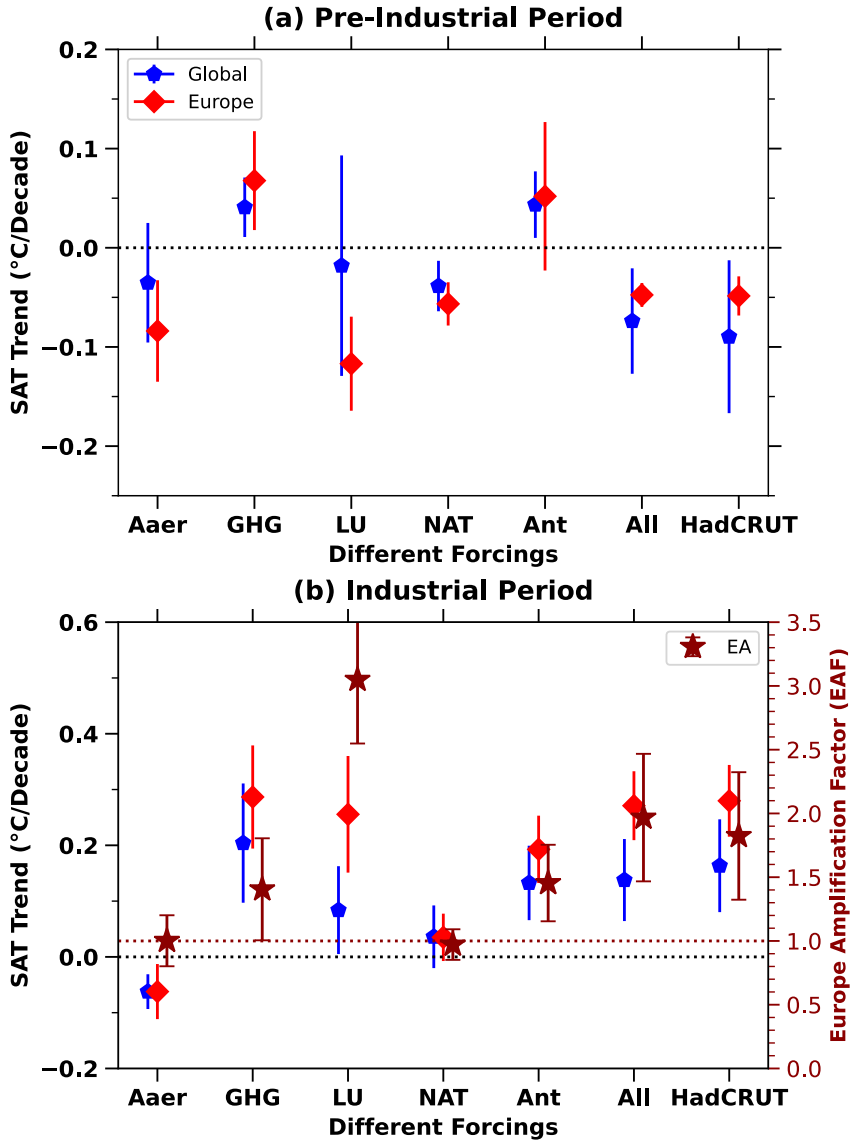


Figure 6. Comparison of urban surface air temperature (SAT) trends and amplification between urban Europe and the global urban mean. Statistically significant SAT trends averaged over urban-influenced regions are shown for Europe and the global domain during the pre-industrial period (1850–1900; panel a) and the industrial period (1955–2005; panel b). Corresponding Europe Amplification Factors (EAF) are shown in panel (b). Red markers indicate European urban SAT trends, while blue markers denote globally averaged urban SAT trends. Brown star symbols represent EAF values (right axis). Only grid points with statistically significant trends are included in the averages; non-significant values are excluded.

reflecting a gradual increase in regional amplification even under moderate forcing levels. The high-emission RCP8.5 scenario (Figure 7j) exhibits a discernible strengthening of amplification during this period, with EAF values approaching ≈1.5 across several highly urbanized zones in western and central Europe. These results suggest that even modest differences in near-term forcing trajectories lead to early divergence in the magnitude of regional amplification, particularly over densely populated regions.

By the mid-future, 2040–2069, amplification intensifies across all scenarios, with the magnitude of EAF increasing systematically with radiative forcing strength. Under RCP2.6 (Figure 7b), EAF values surpass 1.5 across large portions of northern and eastern Europe, though some moderation persists over southern regions. In RCP4.5 and RCP6.0 (Figures 7e and 7h), amplification becomes spatially widespread, with continental-scale EAF values commonly ranging between 1.5 and 2.0. The highest mid-century amplification occurs under RCP8.5 (Figure 7k), where values exceed 2.0 across extensive areas of central and northern Europe. The

21698996, 2026, 20, Downloaded from https://agupubs.onlinelibrary.wiley.com/doi/10.1029/2026JD046541 by Oxford University, Wiley Online Library on [27/10/2026]. See the Terms and Conditions (https://onlinelibrary.wiley.com/terms-and-conditions) on Wiley Online Library for rules of use; OA articles are governed by the applicable Creative Commons License

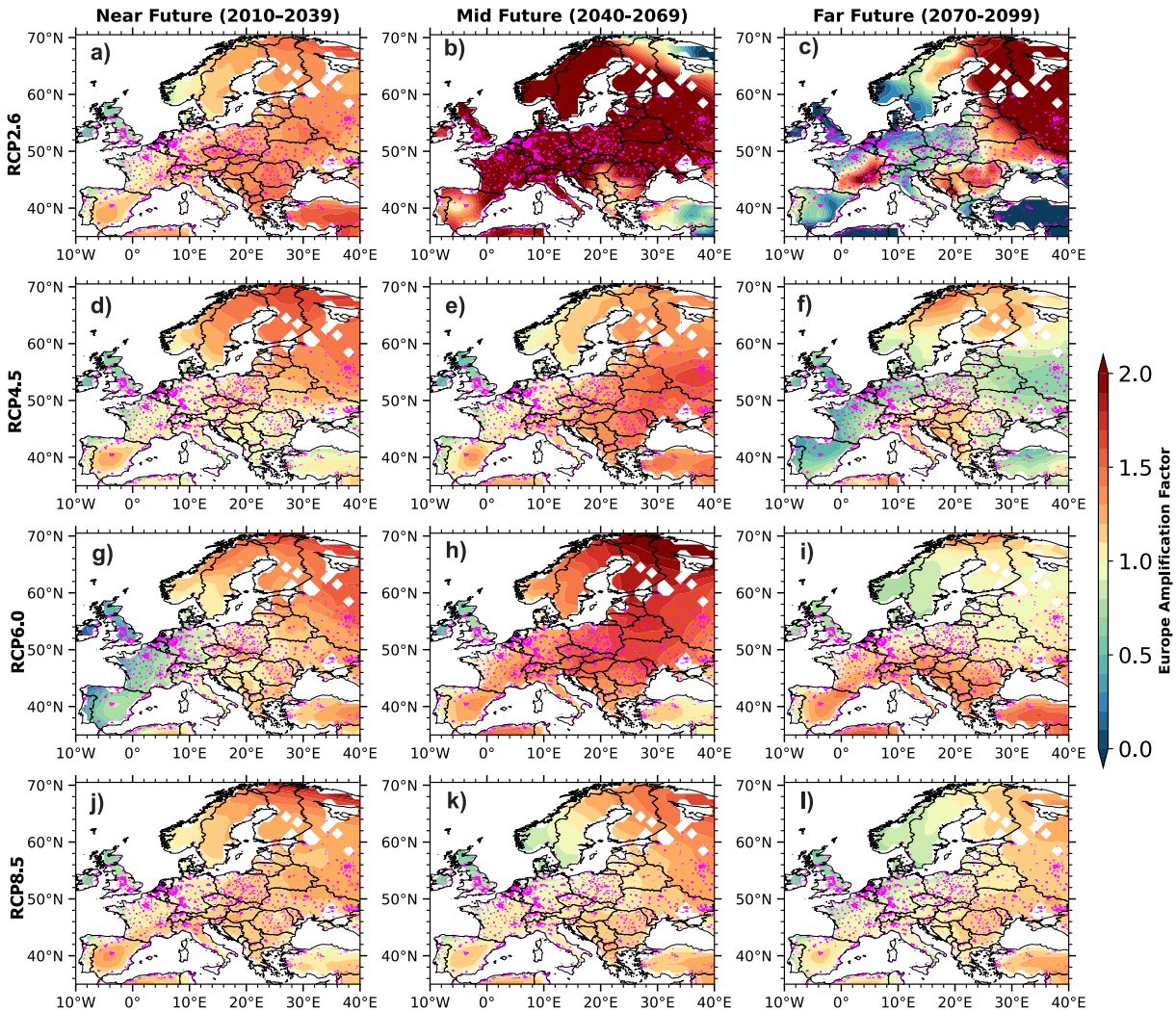


Figure 7. Projected spatial distribution of the Europe Amplification Factor (EAF) under different emission scenarios. EAF patterns over Europe are shown for near future (2010–2039), mid future (2040–2069), and far future (2070–2099) periods under (a) RCP2.6, (b) RCP4.5, (c) RCP6.0, and (d) RCP8.5 scenarios. The EAF is defined as the ratio of regional to global (urban) surface air temperature trends. Values greater than unity indicate amplified warming relative to the global baseline. The colored background represents EAF values across the full European domain and does not denote urban classification. Magenta markers indicate the urban-influenced grid cells identified from the SEDAC population distribution for 2010.

pronounced amplification observed under these scenarios reflects the increasing disparity between local and global SAT trends, indicating that Europe's warming will continue to outpace the global average through mid-century. The spatial coincidence between elevated EAF values and major urban regions underscores the role of land-surface feedbacks and human-driven heat fluxes in modulating regional temperature responses.

In the far-future (2070–2099), the amplification trajectories diverge sharply across the RCP pathways, reflecting the long-term influence of emission intensity on regional climate feedbacks. Under RCP2.6 (Figure 7c), EAF values decline toward near-unity (≈1.0) as global temperatures stabilize under aggressive mitigation, implying limited additional regional divergence from the global mean. However, under intermediate pathways (RCP4.5 and RCP6.0; Figures 7f–7i), strong amplification persists over northern and eastern Europe, with EAF values remaining within the 1.5–2.0 range. Southern Europe, in contrast, exhibits localized reductions in amplification (<1.0), potentially associated with aerosol feedbacks, altered radiation balance, and soil-moisture limitations in semi-arid regions. The high-emission RCP8.5 projection (Figure 7l) reveals the most pronounced and spatially extensive amplification signal, with EAF values reaching up to 2.0 or higher across large swaths of northern and central Europe, as well as over major urban and industrialized regions. This enhanced amplification under sustained high-emission conditions highlights the strong nonlinear response of European SAT trends to radiative

21698996, 2026, 20, Downloaded from https://agupubs.onlinelibrary.wiley.com/doi/10.1029/2026JD046541 by Oxford University, Wiley Online Library on [27/10/2026]. See the Terms and Conditions (https://onlinelibrary.wiley.com/terms-and-conditions) on Wiley Online Library for rules of use; OA articles are governed by the applicable Creative Commons License

21698996, 2026, 20, Downloaded from https://agupubs.onlinelibrary.wiley.com/doi/10.1029/2026JD046541 by Oxford University, Wiley Online Library on [27/10/2026]. See the Terms and Conditions (https://onlinelibrary.wiley.com/terms-and-conditions) on Wiley Online Library for rules of use; OA articles are governed by the applicable Creative Commons License

forcing and the persistence of land-surface feedbacks even under progressive warming. The persistence of high EAF values under RCP6.0 and RCP8.5 underscores the potential for continued regional divergence from global trends and the heightened exposure of European cities to extreme heat stress. These results highlight that achieving meaningful mitigation of regional warming will require an integrated approach that couples emission reduction strategies with targeted land-use management and urban adaptation planning.

4. Conclusion and Discussion

This study provides quantitative evidence that urban Europe's accelerated warming relative to the global mean arises from a coupled atmospheric–surface response. By isolating the effects of greenhouse gases, anthropogenic aerosols, and land-use change, we find that urban Europe has warmed nearly twice as fast as the global average since 1850. The Europe Amplification Factor (EAF) indicates that LU forcing has intensified approximately threefold relative to the global mean (EAF $\approx$ 3.0), while GHG forcing contributes a slightly lower amplification (EAF $\approx$ 2.0). These results demonstrate that Europe's regional warming cannot be explained by atmospheric composition alone, but must also account for large-scale land-surface transformations.

The magnitude of LU-driven amplification reflects the persistent alteration of the surface energy balance caused by urban expansion, vegetation loss, and increased imperviousness. Reduced albedo and evapotranspiration, combined with enhanced sensible heat storage, increase near-surface temperature trends by approximately 0.15–0.25 °C decade^{-1}, compared to ~0.4 °C decade^{-1} under GHG forcing alone. The strong spatial correspondence between high EAF values and densely populated regions, such as the Rhine–Ruhr, Benelux, and Po Valley, illustrates that urbanization has become a dominant amplifier of anthropogenic warming across Europe.

The temporal evolution of these drivers highlights the interplay between GHG forcing, declining aerosol cooling, and intensifying LU feedbacks. Mid-20th-century aerosol emissions temporarily offset GHG-induced warming by up to ~0.15 °C decade^{-1}, but post-1970 clean-air policies removed this cooling mask, exposing the full magnitude of GHG and LU-driven warming. The resulting post-1970 acceleration in observed urban European surface air temperature therefore represents a coupled atmospheric–surface amplification that current climate models tend to underestimate due to coarse spatial resolution and limited representation of urban processes.

Future projections indicate persistent amplification across Europe under moderate to high emission scenarios. Under RCP6.0 and RCP8.5, EAF values remain above 2.0 over central and northern Europe through 2100, with localized peaks exceeding 2.5 in major metropolitan regions. Even under strong mitigation (RCP2.6), EAF values remain within 1.2–1.5, suggesting that Europe's regional divergence from global mean warming will persist throughout the century.

Further, the interpretation of land-use (LU)–driven temperature changes requires careful consideration of competing biogeophysical processes. In CMIP5, LU forcing is dominated by transitions such as forest-to-cropland and pasture conversion, which generally increase surface albedo and can induce a cooling tendency, particularly in temperate and boreal regions (Hurtt et al., 2011). At the same time, these changes reduce evapotranspiration and modify surface roughness, leading to decreased latent heat flux and enhanced sensible heating, which can contribute to warming (Winckler et al., 2019). The net temperature response therefore reflects the balance between these opposing effects and varies regionally. Accordingly, the LU-driven amplification identified in this study should be interpreted as the outcome of combined surface energy balance changes, rather than being attributed to a single mechanism such as albedo reduction alone. In addition to this, the response of surface air temperature to land-use forcing is not governed solely by local surface processes, but also by coupled atmospheric feedbacks (Lawrence et al., 2016). Changes in land cover can modify boundary-layer dynamics, cloud formation, and regional circulation, which may amplify or dampen the direct biogeophysical effects of albedo and surface flux changes (Winckler et al., 2019). In some regions, these atmospheric adjustments can play a dominant role in shaping the net temperature response (Winckler et al., 2019). In addition, it is important to consider that CMIP5 models have been shown to underestimate observed warming over parts of Europe, particularly in regions with strong local feedbacks. Such biases may influence the magnitude of simulated LU-driven amplification and its future projections. Therefore, the results presented here should be interpreted in the context of these uncertainties, reflecting the combined influence of land-surface processes, atmospheric feedbacks, and model limitations.

21698996, 2026, 20, Downloaded from https://agupubs.onlinelibrary.wiley.com/doi/10.1029/2026JD046541 by Oxford University, Wiley Online Library on [27/10/2026]. See the Terms and Conditions (https://onlinelibrary.wiley.com/terms-and-conditions) on Wiley Online Library for rules of use; OA articles are governed by the applicable Creative Commons License

Overall, the rapid and spatially heterogeneous warming over urban Europe reflects the combined influence of atmospheric forcing and anthropogenic land transformation. As illustrated in the conceptual schematic (Figure S3 in Supporting Information S1), different forcing agents contribute through distinct radiative and biogeophysical pathways. The strong LU-driven amplification (EAF $\approx$ 3.0) underscores that emission reductions alone will be insufficient to curb regional warming. Effective urban climate adaptation will therefore require integrated strategies that combine emission mitigation with sustainable land-use planning, enhancement of urban vegetation, and improved infrastructure design, to counteract the persistent influence of surface feedbacks on Europe's amplified climate response.

Inclusion in Global Research Statement

B.S. designed the study, performed the data analysis, and drafted the manuscript. R.G.G., and R.S contributed to the drafting of the manuscript.

Conflict of Interest

The authors declare no conflicts of interest relevant to this study.

Availability Statement

All the data sets and software used in this study are publicly available. All the CMIP5 model data sets are available at (Taylor et al., 2012). Observational data from HadCRUT5 is available at (Morice et al., 2021). SEDAC population data at (Gao, 2020). For visualization, the open-source Python 3.5.0 version was used and is available at (Sanner, 1999).

Acknowledgments
We thank the various platforms for making the data public, such as CMIP5, HadCRUT5 data sets. This study was funded by UK Research and Innovation (UKRI-0771). This study was funded as part of NERC's support of the National Centre for Earth Observation (NE/R016518/1).

References

Barbosa, R., Vicente, R., & Santos, R. (2015). Climate change and thermal comfort in southern Europe housing: A case study from Lisbon. *Building and Environment*, *92*, 440–451. https://doi.org/10.1016/j.buildenv.2015.05.019

Bevacqua, E., Rakovec, O., Schumacher, D. L., Kumar, R., Thober, S., Samaniego, L., et al. (2024). Direct and lagged climate change effects intensified the 2022 European drought. *Nature Geoscience*, *17*(11), 1100–1107. https://doi.org/10.1038/s41561-024-01559-2

Eijkelenboom, A., Tenpierik, M., Ottele, M., Vogt, M., Isabella, O., Cavallo, R., & Bluyssen, P. (2024). Thermal and indoor air quality in dwellings in Europe during summer. *Indoor Environments*.

Etheridge, D. M., Steele, L., Langenfelds, R. L., Francey, R. J., Barnola, J.-M., & Morgan, V. (1996). Natural and anthropogenic changes in atmospheric CO_2 over the last 1000 years from air in Antarctic ice and firn. *Journal of Geophysical Research*, *101*(D2), 4115–4128. https://doi.org/10.1029/95jd03410

Eyring, V., Bony, S., Meehl, G. A., Senior, C. A., Stevens, B., Stouffer, R. J., & Taylor, K. E. (2016). Overview of the coupled model intercomparison project phase 6 (CMIP6) experimental design and organization. *Geoscientific Model Development*, *9*(5), 1937–1958. https://doi.org/10.5194/gmd-9-1937-2016

Falchetta, G., De Cian, E., Sue Wing, I., & Carr, D. (2024). Global projections of heat exposure of older adults. *Nature Communications*, *15*(1), 3678. https://doi.org/10.1038/s41467-024-47197-5

Fastl, C., Arnberger, A., Gallistl, V., Stein, V. K., & Dorner, T. E. (2024). Heat vulnerability: Health impacts of heat on older people in urban and rural areas in Europe. *Wiener Klinische Wochenschrift*, *136*(17), 507–514. https://doi.org/10.1007/s00508-024-02419-0

Gao, J. (2020). Global 1-km downscaled population base year and projection grids based on the shared socioeconomic pathways, revision 01 [Dataset]. *NASA Socioeconomic Data and Applications Center (SEDAC)*. Retrieved from https://www.earthdata.nasa.gov/data/catalog/sedac-ciesin-sedac-pd-sspbsyr-1km-1.01

Gavurova, B., Rigelsky, M., & Ivankova, V. (2021). Greenhouse gas emissions and health in the countries of the European Union. *Frontiers in Public Health*, *9*, 756652. https://doi.org/10.3389/fpubh.2021.756652

Gillett, N. P., Kirchmeier-Young, M., Ribes, A., Shiogama, H., Hegerl, G. C., Knutti, R., et al. (2021). Constraining human contributions to observed warming since the pre-industrial period. *Nature Climate Change*, *11*(3), 207–212. https://doi.org/10.1038/s41558-020-00965-9

Guerreiro, S. B., Dawson, R. J., Kilsby, C., Lewis, E., & Ford, A. (2018). Future heat-waves, droughts and floods in 571 European cities. *Environmental Research Letters*, *13*(3), 034009. https://doi.org/10.1088/1748-9326/aaaad3

Holland, P. W., & Welsch, R. E. (1977). Robust regression using iteratively reweighted least-squares. *Communications in Statistics - Theory and Methods*, *6*(9), 813–827. https://doi.org/10.1080/03610927708827533

House-Peters, L. A., & Chang, H. (2011). Modeling the impact of land use and climate change on neighborhood-scale evaporation and nighttime cooling: A surface energy balance approach. *Landscape and Urban Planning*, *103*(2), 139–155. https://doi.org/10.1016/j.landurbplan.2011.07.005

Hurtt, G. C., Chini, L. P., Frolking, S., Betts, R., Feddema, J., Fischer, G., et al. (2011). Harmonization of land-use scenarios for the period 1500–2100: 600 years of global gridded annual land-use transitions, wood harvest, and resulting secondary lands. *Climatic Change*, *109*(1), 117–161. https://doi.org/10.1007/s10584-011-0153-2

Kishore, P., Basha, G., Venkat Ratnam, M., Velicogna, I., Ouarda, T. B., & Narayana Rao, D. (2016). Evaluating CMIP5 models using GPS radio occultation cosmic temperature in UTLS region during 2006–2013: Twenty-first century projection and trends. *Climate Dynamics*, *47*(9–10), 3253–3270. https://doi.org/10.1007/s00382-016-3024-8

Lauwaet, D., Berckmans, J., Hooyberghs, H., Wouters, H., Driesen, G., Lefebre, F., & De Ridder, K. (2024). High resolution modelling of the urban heat island of 100 European cities. *Urban Climate*, *54*, 101850. https://doi.org/10.1016/j.uclim.2024.101850

Lawrence, D. M., Hurtt, G. C., Arneth, A., Brovkin, V., Calvin, K. V., Jones, A. D., et al. (2016). The land use model intercomparison project (LUMIP) contribution to CMIP6: Rationale and experimental design. *Geoscientific Model Development*, *9*(9), 2973–2998. https://doi.org/10.5194/gmd-9-2973-2016

Masson-Delmotte, V., Zhai, P., Pörtner, H.-O., Roberts, D., Skea, J., Shukla, P. R., et al. (Eds.). (2018). *Global warming of 1.5°C: An IPCC special report on the impacts of global warming of 1.5°C above pre-industrial levels and related global greenhouse gas emission pathways, in the context of strengthening the global response to the threat of climate change, sustainable development, and efforts to eradicate poverty*. Cambridge University Press. https://doi.org/10.1017/9781009157940

Mishra, P., Singh, U., Pandey, C. M., Mishra, P., & Pandey, G. (2019). Application of student's t-test, analysis of variance, and covariance. *Annals of Cardiac Anaesthesia*, *22*(4), 407–411. https://doi.org/10.4103/aca.aca_94_19

Morice, C. P., Kennedy, J. J., Rayner, N. A., Winn, J., Hogan, E., Killick, R., et al. (2021). An updated assessment of near-surface temperature change from 1850: The hadcrut5 data set [Dataset]. *Journal of Geophysical Research: Atmospheres*, *126*(3), e2019JD032361. https://doi.org/10.1029/2019jd032361

Mulville, M., Harrington, S., Li, C., Raushan, K., Essien-Thompson, E., & Ahern, C. (2025). Dwelling overheating in risk in cool climates: Assessing the risk in the context of retrofit and climate change in Ireland. *Indoor Environments*, *2*(1), 100072. https://doi.org/10.1016/j.indenv.2025.100072

Pardo, S. K., & Paredes-Fortuny, L. (2024). Uneven evolution of regional European summer heatwaves under climate change. *Weather and Climate Extremes*, *43*, 100648. https://doi.org/10.1016/j.wace.2024.100648

Philipona, R., Behrens, K., & Ruckstuhl, C. (2009). How declining aerosols and rising greenhouse gases forced rapid warming in Europe since the 1980s. *Geophysical Research Letters*, *36*(2). https://doi.org/10.1029/2008gl036350

Quaranta, E., Dorati, C., & Pistocchi, A. (2021). Water, energy and climate benefits of urban greening throughout Europe under different climatic scenarios. *Scientific Reports*, *11*(1), 12163. https://doi.org/10.1038/s41598-021-88141-7

Sahani, J., Kumar, P., & Debele, S. E. (2024). Assessing demographic and socioeconomic susceptibilities to heatwaves in the southeastern United Kingdom. *Sustainable Cities and Society*, *117*, 105958. https://doi.org/10.1016/j.scs.2024.105958

Sanner, M. F. (1999). Python: A programming language for software integration and development [Software]. *Journal of Molecular Graphics and Modelling*, *17*(1), 57–61. Retrieved from https://www.python.org/

Santamouris, M., & Kolokotsa, D. (2015). On the impact of urban overheating and extreme climatic conditions on housing, energy, comfort and environmental quality of vulnerable population in Europe. *Energy and Buildings*, *98*, 125–133. https://doi.org/10.1016/j.enbuild.2014.08.050

Schulzweida, U., Kornblueh, L., & Quast, R. (2019). CDO user guide.

Schumacher, D. L., Singh, J., Hauser, M., Fischer, E. M., Wild, M., & Seneviratne, S. I. (2024). Exacerbated summer European warming not captured by climate models neglecting long-term aerosol changes. *Communications Earth & Environment*, *5*(1), 182. https://doi.org/10.1038/s43247-024-01332-8

Shaw, B. J., Van Vliet, J., & Verburg, P. H. (2020). The peri-urbanization of Europe: A systematic review of a multifaceted process. *Landscape and Urban Planning*, *196*, 103733. https://doi.org/10.1016/j.landurbplan.2019.103733

Shen, P., Zhao, S., & Ma, Y. (2021). Perturbation of urbanization to earth's surface energy balance. *Journal of Geophysical Research: Atmospheres*, *126*(8), e2020JD033521. https://doi.org/10.1029/2020jd033521

Shen, P., Zhao, S., Ma, Y., & Liu, S. (2023). Urbanization-induced earth's surface energy alteration and warming: A global spatiotemporal analysis. *Remote Sensing of Environment*, *284*, 113361. https://doi.org/10.1016/j.rse.2022.113361

Shiogama, H., Stone, D. A., Nagashima, T., Nozawa, T., & Emori, S. (2013). On the linear additivity of climate forcing-response relationships at global and continental scales. *International Journal of Climatology*, *33*(11), 2542–2550. https://doi.org/10.1002/joc.3607

Swain, B., Vountas, M., Singh, A., Panda, U., Song, R., Anchan, N. L., et al. (2026). Contrasting anthropogenic drivers behind asymmetric warming in the arctic and Antarctica. *Ocean-Land-Atmosphere Research*, *5*, 0127. https://doi.org/10.34133/olar.0127

Taylor, K. E., Stouffer, R. J., & Meehl, G. A. (2012). An overview of CMIP5 and the experiment design [Dataset]. *Bulletin of the American Meteorological Society*, *93*(4), 485–498. https://doi.org/10.1175/bams-d-11-00094.1

Trlica, A., Hutyra, L., Schaaf, C., Erb, A., & Wang, J. (2017). Albedo, land cover, and daytime surface temperature variation across an urbanized landscape. *Earth's Future*, *5*(11), 1084–1101. https://doi.org/10.1002/2017ef000569

van Oldenborgh, G. J., Drijfhout, S., Van Ulden, A., Haarsma, R., Sterl, A., Severijns, C., et al. (2009). Western Europe is warming much faster than expected. *Climate of the Past*, *5*(1), 1–12. https://doi.org/10.5194/cp-5-1-2009

Van Vuuren, D. P., Edmonds, J., Kainuma, M., Riahi, K., Thomson, A., Hibbard, K., et al. (2011). The representative concentration pathways: An overview. *Climatic Change*, *109*(1–2), 5–31. https://doi.org/10.1007/s10584-011-0148-z

Vautard, R., Gobiet, A., Sobolowski, S., Kjellström, E., Stegehuis, A., Watkiss, P., et al. (2014). The European climate under a 2 c global warming. *Environmental Research Letters*, *9*(3), 034006. https://doi.org/10.1088/1748-9326/9/3/034006

Walkowiak, M. P., Bandurski, K., Walkowiak, J., & Walkowiak, D. (2025). Outpacing climate change: Adaptation to heatwaves in Europe. *International Journal of Biometeorology*, *69*(5), 989–1002. https://doi.org/10.1007/s00484-025-02872-0

Ward, K., Lauf, S., Kleinschmit, B., & Endlicher, W. (2016). Heat waves and urban heat islands in Europe: A review of relevant drivers. *Science of the Total Environment*, *569*, 527–539. https://doi.org/10.1016/j.scitotenv.2016.06.119

Wendisch, M., Stapf, J., Becker, S., Ehrlich, A., Jäkel, E., Klingebiel, M., et al. (2023). Effects of variable ice–ocean surface properties and air mass transformation on the arctic radiative energy budget. *Atmospheric Chemistry and Physics*, *23*(17), 9647–9667. https://doi.org/10.5194/acp-23-9647-2023

Winckler, J., Reick, C. H., Luyssaert, S., Cescatti, A., Stoy, P. C., Lejeune, Q., et al. (2019). Different response of surface temperature and air temperature to deforestation in climate models. *Earth System Dynamics*, *10*(3), 473–484. https://doi.org/10.5194/esd-10-473-2019

WMO. (2022). Temperatures in Europe increase at more than twice the global average. Retrieved from https://wmo.int/news/media-centre/temperatures-europe-increase-more-twice-global-average

Wu, X., Wang, J., Ge, Y., Lai, S., Zhang, D., Ren, Z., & Wang, J. (2025). Future heat-related mortality in Europe driven by compound day-night heatwaves and demographic shifts. *Nature Communications*, *16*(1), 7420. https://doi.org/10.1038/s41467-025-62871-y

Yang, H. (2013). The case for being automatic: Introducing the automatic linear modeling (linear) procedure in SPSS statistics. *Multiple Linear Regression Viewpoints*, *39*(2), 27–37.

Zanasi, F., & Keivabu, R. C. (2024). *Extreme temperatures and morbidity in old age in Europe* (Vol. 2024). Vienna Yearbook of Population Research.

21698996, 2026, 20, Downloaded from https://agupubs.onlinelibrary.wiley.com/doi/10.1029/2026JD046541 by Oxford University, Wiley Online Library on [27/10/2026]. See the Terms and Conditions (https://onlinelibrary.wiley.com/terms-and-conditions) on Wiley Online Library for rules of use; OA articles are governed by the applicable Creative Commons License